Accepted Manuscript

Flexure of continuous HSC beams with external CFRP tendons: Effects of fibre elastic modulus and steel ratio

Tiejiong Lou, Sergio M.R. Lopes, Adelino V. Lopes

Flexure of continuous HSC beams with external CFRP tendons: Effects of fibre elastic modulus and steel ratio

Tiejiong Lou[1], Sergio M. R. Lopes[*1], Adelino V. Lopes[2]

1. CEMUC, Department of Civil Engineering, University of Coimbra, Coimbra 3030-788, Portugal
2. Department of Civil Engineering, University of Coimbra, Coimbra 3030-788, Portugal
(*) – Corresponding author, email: sergio@dec.uc.pt

Abstract: The results of a theoretical study on the flexural behaviour of continuous high-strength concrete (HSC) beams prestressed with external fibre reinforced polymer (FRP) tendons are presented. A previously developed numerical model is extended to the analysis of continuous HSC beams with external FRP tendons. A numerical test is conducted on two-span externally prestressed beams made of HSC with compressive strength of 90 MPa. The external tendons are assumed to be Carbon FRP (CFRP) composites covering a wide range of modulus of elasticity. Various levels of nonprestressed steel ratio are used. Comprehensive aspects of behaviour of such type of beams are examined. The results show that CFRP with high elastic modulus of 500 GPa mobilizes quite different structural responses compared to those with normal elastic modulus, and that the amount of nonprestressed steel affects remarkably the behaviour of such beams. The study also indicates that some moment redistribution knowledge valid for conventional continuous concrete beams may not be applicable to continuous HSC beams with external FRP tendons.

Keywords: Continuous beam; External prestressing; Flexural behaviour; Fibre reinforced polymer; High-strength concrete

1. Introduction

External prestressing has been very common in application to either the strengthening or the construction of multi-span concrete girder bridges. Such type of structures, where the strength and durability are of particular importance, is often made of high-strength concrete (HSC). Although HSC is more fragile than normal-strength concrete (NSC), the ductile behaviour of HSC members may not be inferior to that of NSC members if a proper choice of the amount and location of steel is made [1-4].

Due to their advantages of non-corrosive property and high tensile strength, fibre reinforced polymer (FRP) composites are widely used in concrete structures instead of conventional steel reinforcement [5-7]. The use of FRP materials as external tendons is expected to be increasingly popular, as these tendons are often exposed to exterior environment and therefore need a very high anticorrosion protection. For external FRP tendon systems, the major concerns arise from the bond at anchorages, since the anchorages in such systems are extremely critical for prestress transfer and interaction between external tendons and the member over the entire life of the structure. Many efforts have been made to the development of safe and reliable anchorage systems for FRP tendons, and some achievements have been reached [8]. Three basic FRP composites are typically available for prestressing tendons, namely, aramid FRP (AFRP), carbon FRP (CFRP) and glass FRP (GFRP) [8-11]. The common GFRP composites have poor resistance to alkaline environment and, therefore, they are not permitted for internal bonded tendons. GFRP composites are

also susceptible to creep rupture under sustained loads and can indefinitely sustain only about 30% of their ultimate strength [12]. AFRP and CFRP are both desirable for prestressed concrete applications, while the latter generally exhibits better mechanical properties than the former [12]. A recent numerical study by the authors [13] showed that the behaviour of concrete beams with external CFRP tendons (having elastic modulus of 147 GPa) is very similar to that of the ones with external steel tendons. This observation is consistent with an experimental study by Bennitz et al. [14].

The accurate analysis of beams prestressed with external tendons is rather complicated, attributed to the lack of compatibility of the strains between external tendons and the adjacent concrete and to the variation in eccentricities of external tendons with varying beam deformations (second-order effects) [15,16]. For continuous HSC beams with external FRP tendons, some additional difficulties arise due to the existence of redundant restraints and the distinctive material properties of HSC and FRP. So far, few theoretical efforts [17,18], as well as a very limited experimental works [19-21], have been carried out to identify the behaviour of continuous external tendon systems, particularly the ones with combined HSC and FRP materials. Because of the lack of experimental data and theoretical studies, the behaviour of continuous HSC beams prestressed with external FRP tendons has yet to be well understood.

This article describes a numerical investigation of flexural behaviour of continuous HSC beams prestressed with external CFRP tendons, focusing on the effects of CFRP modulus of elasticity and nonprestressed steel ratio. Comprehensive

aspects of behaviour of such beams are evaluated, including the stress increase in external tendons, the curvature ductility, the variation of neutral axis depth, the redistribution of moments, and the failure mode and crack pattern. The present numerical study is performed using a finite element model developed specifically for externally post-tensioned beams.

2. Method of numerical analysis

A finite element model for the full-range nonlinear analysis of externally prestressed concrete beams has been developed [22]. The basic assumptions adopted are: a plane section remains plane after deformations; nonprestressed steel completely bonds with the surrounding concrete; the frictions between deviators and external tendons are negligible; and the shear deformation is negligible. The numerical method is formulated based on the Euler-Bernoulli beam theory combined with the layered approach. According to the updated Lagrangian description, the stiffness matrix consists of the material stiffness matrix, which represents the material nonlinear effect, and the geometric stiffness matrix, which represents the large displacement effect. At each step during the solution process, the geometry (length and eccentricities) of external tendons are updated in terms of the current nodal displacements of beam elements (anchorage and deviator points are associated with the corresponding beam element nodes). The increment in tendon strain is calculated from the elongation of the entire tendon. The contribution of external prestressing to the concrete beam is made by transforming the current prestressing force into equivalent loads acting on

4

the finite element model. Details of the numerical treatment of external or unbonded tendons can be seen in the references [22,23]. A load control or displacement control incremental method, together with the Newton-Raphson iterative algorithm, is used to trace the structural equilibrium path throughout the elastic, nonlinear and ultimate ranges. During the solution process, when the concrete strain at the critical section reaches the allowed maximum strain, the beam is assumed to be crushed.

In the finite element idealization, the concrete beam is divided into two-node beam elements and the external tendon is also divided into segments corresponding to the beam elements. The spacing between adjacent nodes is dependent on the precision requirement for an analysis; generally, a spacing of one-half to two times (smaller at critical regions and larger at noncritical regions) the cross-sectional depth is acceptable. Each element is subdivided into a number of concrete and reinforcement layers to include the different material properties across the depth of the section. The number of layers relies on the section shape; in general, 10, 12 and 16 concrete layers can be respectively used for rectangular, T- and I-beams.

The previously developed model [22], however, is limited to the analysis of NSC beams prestressed with external steel tendons, because the constitutive laws introduced in the model are valid only for NSC and steel materials. These laws are inadequate to simulate the behaviour of HSC and FRP materials. To allow the proposed numerical method to predict the behaviour of continuous HSC beams prestressed with external FRP tendons, the following material models are adopted in the present study:

The stress-strain relationship for concrete in compression recommended by Eurocode 2 [24] has been proved to be applicable to both NSC and HSC, and is adopted here. It is expressed as follows:

$$\frac{\sigma_c}{f_{cm}} = \frac{k\eta - \eta^2}{1 + (k-2)\eta} \tag{1}$$

where $\eta = \varepsilon_c / \varepsilon_{c0}$; σ_c and ε_c are the concrete stress and strain, respectively; $k = 1.05 E_c \varepsilon_{c0} / f_{cm}$; ε_{c0} is the concrete strain at peak stress, and $\varepsilon_{c0}(\text{‰}) = 0.7 f_{cm}^{0.31}$; E_c is the modulus of elasticity of concrete (in GPa), and $E_c = 22(f_{cm}/10)^{0.3}$; f_{cm} is the mean compressive strength (in MPa), and $f_{cm} = f_{ck} + 8$; f_{ck} is the characteristic cylinder compressive strength (in MPa). Eq. (1) is subject to the condition that the concrete strain is not greater than the ultimate compressive strain ε_u, which for HSC is determined by

$$\varepsilon_u(\text{‰}) = 2.8 + 27[(98 - f_{cm})/100]^4 \tag{2}$$

The stress-strain diagram for concrete in tension is assumed to be composed of a linearly ascending branch before cracking and a linearly descending branch after cracking up to zero stress, as indicated by

Prior to cracking, $\qquad\qquad \sigma_c = E_c \varepsilon_c \tag{3a}$

After cracking, $\qquad \sigma_c = f_t \left[1 - \dfrac{\varepsilon_c - \varepsilon_{cr}}{\varepsilon_{tu} - \varepsilon_{cr}} \right] \tag{3b}$

where f_t = concrete tensile strength ; ε_{cr} = f_t/E_c; and ε_{tu} = concrete tensile strain corresponding to zero stress. When the concrete strain is greater than ε_{tu}, the tensile stress is equal to zero. According to Eurocode 2 [24], the tensile strength f_t for HSC is calculated from

6

$$f_t = 2.12 \ln(1 + f_{cm}/10) \tag{4}$$

The prestressing FRP tendons are linearly elastic up to rupture and, therefore, the stress σ_f is related to the strain ε_f by

Prior to rupture, $\qquad\qquad\qquad \sigma_f = E_f \varepsilon_f \qquad\qquad\qquad$ (5a)

After rupture, $\qquad\qquad\qquad \sigma_f = 0 \qquad\qquad\qquad$ (5b)

where E_f = FRP tendon modulus of elasticity. The nonprestressed steel is assumed to be elastic-perfectly plastic in both tension and compression.

A computer programme incorporating the aforementioned numerical procedure and material models was written. The programme is able to take care of simply supported and continuous beams made of NSC and HSC and prestressed with external steel and FRP tendons, under symmetrical and unsymmetrical loading. It requires the input of geometry and boundary condition, loading data, material properties, etc. The output includes nodal displacements (axial, transverse displacements and rotation), support reactions; section moments and curvatures; stresses and strains in external tendons, nonprestressed steel and concrete.

In order to validate the proposed model, six two-span continuous externally post-tensioned beams tested by Harajli et al. [19] have been investigated. These beams were B6D1, B6D2, B12D1 B12D2, B10S1A and B10S1B. The experimental and computational values of the ultimate load and ultimate tendon stress are given in Table 1. Fairly good agreement can be observed for the specimens. The average discrepancy for the ultimate load is -0.5%, with a standard deviation of 2.4%; and the average discrepancy for the ultimate tendon stress is 5.6%, with a standard deviation

7

of 5.7%. The comparison between the numerical and exprimental results ragarding the load-deflection curve and the response of load versus stress increase in external tendons has been reported elsewhere [18].

3. Numerical test

A numerical test is conducted using the above described nonlinear model to study the flexural behaviour of continuous HSC beams prestressed with external FRP tendons. The aspects of behaviour examined include the stress increase in external tendons, the curvature ductility, the variation of neutral axis depth, the redistribution of moments, and the failure mode and crack pattern. The investigation variables include the modulus of elasticity of FRP tendons and the ratio of nonprestressed steel.

An externally prestressed HSC rectangular beam continuous over two equal spans to which two centre-point loads are symmetrically applied, as shown in Fig. 1(a), is used as a control beam for the numerical evaluation. In Fig. 1(a), A_{s1}, A_{s2} and A_{s3} represent the areas of nonprestressed tensile steel over positive moment region, negative moment region and nonprestressed compressive steel, respectively. The nonprestressed steel contents are as follows: A_{s3} = 400 mm^2; A_{s2} = 400 ~ 4800 mm^2; and ρ_{s2}/ρ_{s1} (or A_{s2}/A_{s1}) = 2/3, where $\rho_{s1} = A_{s1}/(bh)$, $\rho_{s2} = A_{s2}/(bh)$, b is the section width and h is the section height. The yield strength and elastic modulus of nonprestressed steel are 450 MPa and 200 GPa, respectively. Since CFRPs cover a wide range of modulus of elasticity, E_f, which may vary between 80 and 500 GPa [25], the external tendons are assumed to be CFRP composites so as to enable a

8

comparative study on various E_f levels. Three types of CFRP composites, designated as CFRP-80, CFRP-147 and CFRP-500, are used. The material properties (tensile strength f_f, elastic modulus E_f, and ultimate strain ε_{fu}) for each type of CFRP tendons are summarized in Table 2. CFRP-80 and CFRP-500 represent the lowest and highest values, respectively, of the modulus of elasticity among CFRP composites. The elastic modulus of CFRP-147 is close to that of the prestressing steel and, therefore, this type of CFRP tendons have been recognized as an ideal material to replace the conventional steel tendons without changing noticeably the structural performance of the beams. The tendon area is taken as 500 mm^2, and the initial prestress is taken as 1050 MPa. The cylinder compressive strength f_{ck} for HSC is taken as 90 MPa.

The finite element model of the beam is shown in Fig. 1(b). The concrete beam is divided into 36 two-node beam elements (18 elements for each span) with length of 555.56 mm each, and the external tendons are also divided into 36 segments corresponding to the beam elements. Each beam element is subdivided into 10 concrete layers and 2 steel layers representing the top and bottom nonprestressed steel, respectively.

4. Results and discussion

4.1. Stress increase in external tendons

Fig. 2 shows the stress increments in external CFRP tendons with the applied load and with the midspan deflection for the beams with ρ_{s2} of 0.44%. It is observed that the increase in tendon stress is trivial at initial loading up to cracking at midspan

9

(second cracking). This is followed by a quick stress increase with increasing load and, after the development of cracks stabilizes, the stress in external tendons increases almost linearly with the applied load until yielding of steel at midspan (second yielding). Beyond that, the tendon stress increases very quickly with a small growth of the applied load up to failure. In these beams analysed, cracking and steel yielding at the centre support (first cracking and first yielding) do not produce noticeable effects on the load versus tendon stress response of continuous beams, attributed to continuity and to relatively lower amount of nonprestressed steel over the centre support region. In addition, it is seen in the graph that at a given load level, in comparison with CFRP-147 tendons, CFRP-500 tendons register a much higher stress increment while CFRP-80 tendons mobilizes a smaller stress increment, attributed to different levels of tendon moduli of elasticity.

Due to elastic behaviour of FRP composites, there is an approximately linear relationship between deflection and tendon stress increment over the entire loading range, as shown in Fig. 2. The slope of the curves depends on the tendon modulus of elasticity. In this analysis, the slopes for CFRP-80, CFRP-147 and CFRP-500 tendons for ρ_{s2} of 0.44% are 1.66, 3.01 and 9.77 MPa/mm, respectively.

Fig. 3 shows the variation of the stress increase in external tendons at ultimate with the nonprestressed steel ratio. It is seen that, as the steel ratio increases, the ultimate stress increment in external tendons decreases except at very low steel ratios (ρ_{s2} below 0.44%) where the phenomenon is opposite. The higher the tendon modulus of elasticity, the higher the tendon stress increment at ultimate. The

difference between the ultimate tendon stress increments in different types of CFRP tendons is notable at a low steel ratio, but tends to diminish with the increase of the steel ratio.

4.2. Moment-curvature response and curvature ductility

Fig. 4 illustrates the moment (absolute value)-curvature responses at the centre support and at midspan for the HSC beams with different types of external CFRP tendons. The results are produced using ρ_{s2} of 0.44%. Before application of live loads, there exist initial moments due to self-weight and secondary reactions. The initial centre support moment is about 1.5 times the initial midspan moment. It should be noted that because the tendon line is below the linearly transformed concordant line, the secondary reaction at the end support is positive and, therefore, the secondary moments are also positive. If the tendon line is linearly transformed into a concordant line so as to minimize the secondary moments, the centre support moment would be higher while the midspan moment would be lower. The complete moment-curvature response for the centre support or midspan section consists of three stages with two turning points corresponding to concrete cracking and tensile steel yielding of the section, respectively. Since the cracking moment of a section is mainly contributed by concrete, the difference between the cracking moments of the centre support section and midspan section is insignificant. After cracking, the contributions of reinforcement become increasingly important. Because the amount of nonprestressed tensile steel over the centre support region is smaller than that over the midspan region, the yielding and ultimate moments of the centre support section are obviously

11

lower than those of the midspan section, as can be seen in Fig. 4.

Prior to cracking, the beams with different types of external CFRP tendons display approximately identical moment-curvature behaviour. After cracking, the CFRP-500 tendon beam is stiffer than the other two beams. Due to higher tendon stress developed at steel yielding and at ultimate, the CFRP-500 tendon beam mobilizes higher yielding and ultimate moments compared to the others.

Although CFRP composites are linear elastic material without yielding, the external CFRP tendon beams may exhibit good ductile behaviour due to the existence of nonprestressed steel, as can be seen in Fig. 4. The flexural ductility of partially prestressed concrete beams may be expressed using the curvature ductility as follows:

$$\mu_\phi = \frac{\phi_u}{\phi_y} \tag{6}$$

where μ_ϕ is the curvature ductility factor; ϕ_u and ϕ_y are the section curvatures at ultimate and at yielding of nonprestressed steel, respectively.

Fig. 5 shows the variation of μ_ϕ of the centre support section and midspan section with the nonprestressed steel ratio for the beams with different types of CFRP tendons. It is generally observed that at a given tendon type, the ductility decreases as the steel ratio increases. However, the ductility of the centre support section has a slight increase when ρ_{s2} increases from 0.22% to 0.44%. It is also seen that with increasing steel ratio, the decrease in the ductility of the midspan section is much quicker than that of the centre support section. At a low steel ratio, the ductility of the midspan section is higher than that of the centre support section, while at a high steel ratio, the phenomenon is opposite. At a low steel ratio, the curvature ductility of

12

CFRP-500 tendon beams is obviously lower than that of CFRP-80 or CFRP-147 tendon beams, while the ductility difference gradually diminishes as the steel ratio increases.

4.3. Variation of neutral axis depth

Before application of any live load, there is a slight sagging curvature at the centre support and hogging curvature at midspan due to the effects of external prestressing. For the beams analysed, the initial neutral axis depths at the centre support and at midspan are negative, that is, the neutral axis lies somewhere below the bottom fibre of the centre support section or above the top fibre of the midspan section. With the application and increase of the live load, the centre support sagging curvature or midspan hogging curvature gradually disappears and, correspondingly, the neutral axis moves downward at the centre support or upward at midspan. When the centre support hogging curvature or midspan sagging curvature begins to appear, the neutral axis jumps suddenly from a place far below the bottom fibre to a place far above the top fibre at the centre support, or from a place far above the top fibre to a place far below the bottom fibre at midspan. With continuing increase of the applied load, the neutral axis moves (drops at the centre support or rises at midspan) rapidly towards the extreme tension fibre of the cross section.

Fig. 6 shows the variation of neutral axis depths at the centre support and at midspan with the applied load, after the neutral axis moves to the extreme tension fibre of the cross section. It is seen that before yielding of the midspan steel, at a given load level, the neutral axis depth at the centre support is obviously lower than

that at midspan. After the midspan steel yields, the shift of the midspan neutral axis is much quicker than that of the centre support one; consequently, the difference between the neutral axis depths for the centre support and midspan sections gradually diminishes. It is also observed that the continuous beams with different types of external CFRP tendons exhibit almost identical load versus neutral axis depth behaviour up to stabilization of the crack development. Beyond that, the neutral axis for the external CFRP-500 tendon beam moves slower than that for the external CFRP-80 or CFRP-147 tendon beam.

After the neutral axis enters into the cross section, the curvature versus neutral axis depth responses for the centre support and midspan sections of the beams with different types of external CFRP tendons are shown in Fig. 7. The shift of the neutral axis is very quick at first, but it tends to slow down as the curvature increases. After the centre support or midspan steel has apparently yielded, the movement of neutral axis of the section becomes very slow. It is also seen that the type of CFRP tendons has insignificant effects on the curvature versus neutral axis depth response.

Fig. 8 illustrates the variation of c/h (ratio of the neutral axis depth at ultimate to the section height) with the nonprestressed steel ratio for the beams with different types of external CFRP tendons. It is seen that the neutral axis depth increases as the steel ratio increases. The rate of increase in the neutral axis depth of the centre support section is much smaller than that of the midspan section. The difference between the neutral axis depths of the centre support and midspan sections is negligible at a low steel ratio, but becomes increasingly obvious with the increase of the steel ratio. At a

14

given steel ratio, CFRP-500 tendons mobilize higher neutral axis depths than do CFRP-80 or CFRP-147 tendons.

4.4. Moment redistribution

In a simply supported beam, the support reaction develops linearly with the applied load over the entire loading range. In a continuous beam, on the other hand, the linear relationship between the applied load and support reaction may be no longer valid when the elastic limit of any constituent material is exceeded, attributed to redistribution of moments. To verify this statement, the development of the end and centre support reactions with the applied load for the continuous beams with different types of external CFRP tendons is illustrated in Fig. 9. Both the actual and elastic values are demonstrated. The actual values are obtained from the nonlinear finite element analysis, while the elastic values are calculated assuming the constituent materials are linear elastic. It is seen that the actual reactions are identical to the elastic values at initial loading up to cracking. Thereafter, the actual reactions begin to deviate from the elastic values due to redistribution of moments. Because the first crack appears at the centre support, on cracking the moments are redistributed towards the span critical region, causing a growth of the rate of increase in the end support reaction, whereas a diminution of the rate of increase in the centre support reaction. Also, it is generally observed that the deviation between the actual and elastic reactions enlarges with increasing load.

The redistribution of moments may be measured in terms of the degree of moment redistribution defined by

$$\beta = 1 - \frac{M}{M_e} \tag{7}$$

where M is the actual moment; and M_e is the moment calculated from an elastic analysis.

Fig. 10 shows the variation of the degrees of moment redistribution at the centre support and at midspan with the applied load for the beams with different types of external CFRP tendons. It is seen that at initial loading up to the appearance of first cracking, there is no redistribution of moments (β = 0). After cracking, the phenomenon of moment redistribution appears, while the redistribution evolution is typically affected by several phases occurring during the loading process. The degree of moment redistribution increases with the applied load until the development of cracks stabilizes. This is followed by a plateau which is ended by yielding of tensile steel at the centre support. Beyond that, the degree of moment redistribution increases again with increasing load up to yielding of tensile steel at midspan. Thereafter, the degree of moment redistribution tends to slightly decrease until the beam fails. In addition, it can be observed that the values of the degree of moment redistribution, developed at two main stages (stage between first cracking and the stabilization of crack development and stage between first and second yielding), for the beams with different types of external tendons are almost identical.

Fig. 11 shows the variation of the degree of moment redistribution at ultimate at the centre support with the steel ratio for the beams with different types of external CFRP tendons. It is seen that, in comparison with the CFRP-147 tendons, CFRP-500 tendons mobilize obvious lower moment redistribution while CFRP-80 tendons

16

register slightly higher moment redistribution. It is also seen that for ρ_{s2} higher than

1.56%, the degree of moment redistribution tends to decrease with the increase of the

steel ratio. On the other hand, for ρ_{s2} not greater than 1.56%, it is surprisingly found

that a higher level of steel ratio leads to considerably higher redistribution of moments.

In this analysis, as ρ_{s2} increases from 0.22% to 1.56%, the degrees of moment

redistribution increase notably by 41.83% for CFRP-80 tendons, by 43.6% for

CFRP-147 tendons and by 49.39% for CFRP-500 tendons. These observations are

interesting because they are quite different from the common knowledge on moment

redistribution. In conventional reinforced concrete members, the degree of moment

redistribution tends to decrease with increasing steel ratio due mainly to the reduction

in the flexural ductility. This statement is reflected in various design codes related to

moment redistribution. However, such common knowledge and design codes can not

be applied to the HSC beams prestressed with external FRP tendons, since the

moment redistribution capacity in such type of beams can be significantly enhanced

by increasing a certain amount of tensile steel, according to the findings of the current

study. Therefore, a reasonable consideration of the particular moment redistribution

behaviour is necessary when designing this new type of external tendon systems.

Further studies are recommended to propose new simplified equations for calculating

the degree of moment redistribution in continuous HSC beams prestressed with

external FRP tendons for practical design purposes.

4.5. Failure mode and crack pattern

In this section, the failure mode and crack pattern of continuous HSC beams with

external CFRP tendons are examined. The results of the beams without any bonded nonprestressed steel are also presented for comparison.

Similar to other experimental observations on externally post-tensioned beam specimens [19,20], failure of all the analysed beams takes place due to crushing of concrete at the critical section. For continuous beams, the most favourable failure mode is to form a collapse mechanism in which all of the critical sections attain the ultimate failure. The failure mode of two-span continuous beams collapsing by crushing of concrete can be reflected by the value of $\varepsilon_{u2}/\varepsilon_{u1}$ (ratio of the concrete strain at the extreme compressive fibre of the centre support section to that of the midspan section). The beam concrete is crushed at midspan when $\varepsilon_{u2}/\varepsilon_{u1}$ is smaller than 1.0, and at the centre support when $\varepsilon_{u2}/\varepsilon_{u1}$ is great than 1.0. When $\varepsilon_{u2}/\varepsilon_{u1}$ is equal to 1.0, the centre support section and midspan section fail concurrently and thereby the most desirable failure mode forms. Fig. 12 demonstrates the variation of $\varepsilon_{u2}/\varepsilon_{u1}$ with the tensile steel ratio for the beams with different types of external CFRP tendons. It is seen that at a low steel ratio, the value of $\varepsilon_{u2}/\varepsilon_{u1}$ is much smaller than 1.0, indicating that the centre support section is still far away from its full capacity when the midspan concrete is crushed. As the steel ratio increases, the value of $\varepsilon_{u2}/\varepsilon_{u1}$ increases, indicating that the utilization of the ability of the centre support section is improved. When ρ_{s2} increases to 2.11%, the value of $\varepsilon_{u2}/\varepsilon_{u1}$ is close to 1.0, indicating an approximately full development of the rotation capacity and deformation ability of the beam. When ρ_{s2} increases continuously to 2.67%, the value of $\varepsilon_{u2}/\varepsilon_{u1}$ turns to be larger than 1.0, indicating that the collapse takes place at

18

the centre support. It is also seen that as compared to the CFRP-80 or CFRP-147 tendon beam, the CFRP-500 tendon beam exhibits a higher $\varepsilon_{u2}/\varepsilon_{u1}$ value and thereby a better exploitation of the centre support section.

Fig. 13 and 14 illustrate the curvature distribution and the concrete strain distribution at extreme compression and tension fibre, respectively, along the length of the beams, x/L (ratio of the distance from the end support to the span), at failure. The crack pattern at ultimate can be deduced from the graphs. For the beam without any bonded steel, there are three main cracks - two around the loading points and one around the centre support, while the other zones of the beam are almost uncracked. The crack width around the loading point is very large, while the crack width around the centre support is relatively much smaller. On the other hand, for the beams containing bonded steel, more cracks form at failure. As the steel ratio increases, the number of cracks increases while the crack width diminishes, and the reduction in the crack width at the span critical section is much more significant than that at the centre support. As a consequence, the crack width at the span critical section turns to be smaller than that at the centre support at a high steel ratio. These observations regarding the influence of nonprestressed steel on the crack pattern are consistent with several experimental studies [19,26,27]. It can also be observed from Fig. 14 that the type of external CFRP tendons has insignificant influence on the crack pattern, attributed to unbonded nature between external tendons and the adjacent concrete. The beams with different types of external CFRP tendons have nearly the same cracking zones, but CFRP-500 tendons mobilize slightly smaller crack widths at the

19

critical sections than do CFRP-80 or CFRP-147 tendons.

5. Conclusions

A numerical study is conducted to examine the flexural behaviour of two-span continuous HSC beams prestressed with external CFRP tendons. Various levels of fibre modulus of elasticity and nonprestressed steel ratio are used for the numerical evaluation. The main conclusions drawn are as follows:

(1) CFRP-500 tendons develop much higher ultimate stress increase and, consequently, mobilize obviously higher ultimate load-carrying capacity but smaller deflection of the beam, compared to CFRP-80 and CFRP-147 tendons. The stress increase in external tendons tends to gradually decrease with the increase of the nonprestressed steel ratio except at very low steel ratios. The decrease rate for external CFRP-500 tendons is faster than that for CFRP-80 or CFRP-147 tendons.

(2) HSC beams prestressed with external FRP tendons can exhibit good ductile behaviour due to the existence the nonprestressed steel. The CFRP-500 tendon beam displays obviously lower curvature ductility than the CFRP-80 or CFRP-147 tendon beam at a low steel ratio, while the difference of the ductility factors by various CFRP tendons tends to diminish with increasing steel ratio.

(3) At a given steel ratio, CFRP-500 tendons mobilize a higher neutral axis depth compared to CFRP-80 or CFRP-147 tendons. The neutral axis depth increases with the increase of the steel ratio. The rate of increase for the centre support section is much smaller than that for the midspan section. The difference between the centre

20

support neutral axis depth and the midspan one is insignificant at a low steel ratio, but becomes increasingly significant as the steel ratio increases.

(4) Moment redistribution takes place with the appearance of the first crack, and its evolution is later affected typically by stabilization of crack development, first and second steel yielding. CFRP-500 tendons mobilize lower moment redistribution than CFRP-80 and CFRP-147 tendons. Some common moment redistribution knowledge valid for conventional reinforced concrete beams may not be applied to HSC beams prestressed with external FRP tendons. In such beams, a higher steel ratio may lead to considerably higher redistribution of moments.

(5) In this analysis, the beam with ρ_{s2} of 2.11% approaches the most desirable failure mode in which the centre support section and midspan section fail concurrently. At failure load, in a beam without any bonded steel, a crack with very large width forms at each of the span critical sections and a crack with relatively much smaller width forms at the centre support, while the other zones remain almost uncracked. Better crack pattern is observed when bonded steel is provided. The effect of the type of external CFRP tendons on the crack pattern is not important.

References

[1] Bernardo LFA, Lopes SMR. Plastic analysis of HSC beams in flexure. Materials and Structures 2009; 42: 51-69.

[2] Kassoul A, Bougara A. Maximum ratio of longitudinal tensile reinforcement in high strength doubly reinforced concrete beams designed according to Eurocode 8. Engineering Structures 2010; 32: 3206-3213.

[3] Arslan G, Cihanli E. Curvature ductility prediction of reinforced high-strength concrete beam sections. Journal of Civil Engineering and Management 2010; 16(4): 462-470.

[4] Bai ZZ, Au FTK. Flexural ductility design of high-strength concrete beams. Structural Design of Tall and Special Buildings 2013; 22(6): 521-542.

[5] Yu B, Kodur VKR. Factors governing the fire response of concrete beams reinforced with FRP rebars. Composite Structures 2013; 100: 257-269.

[6] Lin X, Zhang YX. Evaluation of bond stress-slip models for FRP reinforcing bars in concrete. Composite Structures 2014; 107: 131-141.

[7] De Domenico D, Pisano AA, Fuschi P. A FE-based limit analysis approach for concrete elements reinforced with FRP bars. Composite Structures 2014; 107: 594-603.

[8] Schmidt JW, Bennitz A, Taljsten B, Goltermann P, Pedersen H. Mechanical anchorage of FRP tendons – A literature review. Construction and Building

Materials 2012; 32: 110-121.

[9] Stoll F, Saliba JE, Casper LE. Experimental study of CFRP-prestressed high-strength concrete bridge beams. Composite Structures 2000; 49: 191-200.

[10] Ghallab A, Beeby AW. Factors affecting the external prestressing stress in externally strengthened prestressed concrete beams. Cement & Concrete Composites 2005; 27: 945-957.

[11] Elrefai A, West J, Soudki K. Fatigue of reinforced concrete beams strengthened with externally post-tensioned CFRP tendons. Construction and Building Materials 2012; 29: 246-256.

[12] ACI Committee 440. Guide for the design and construction of externally bonded FRP systems for strengthening concrete structures. ACI 440.2R-08, American Concrete Institute, Farmington Hills, MI; 2008.

[13] Lou TJ, Lopes SMR, Lopes AV. Numerical analysis of behaviour of concrete beams with external FRP tendons. Construction and Building Materials 2012; 35: 970-978.

[14] Bennitz A, Schmidt JW, Nilimaa J, Taljsten B, Goltermann P, Ravn DL. Reinforced concrete T-beams externally prestressed with unbonded carbon fiber-reinforced polymer tendons. ACI Structural Journal 2012; 109(4): 521-530.

[15] Harajli M, Khairallah N, Nassif H. Externally prestressed members: Evaluation of second-order effects. ASCE Journal of Structural Engineering 1999; 125(10): 1151-1161.

[16] Lou TJ, Xiang YQ. Numerical analysis of second-order effects of externally

23

prestressed concrete beams. Structural Engineering and Mechanics 2010; 35(5): 631-643.

[17] Kim KS, Lee DH. Nonlinear analysis method for continuous post-tensioned concrete members with unbonded tendons. Engineering Structures 2012; 40: 487-500.

[18] Lou TJ, Lopes SMR, Lopes AV. Flexural response of continuous concrete beams prestressed with external tendons. ASCE Journal of Bridge Engineering 2013; 18(6): 525-537.

[19] Harajli MH, Mabsout ME, Al-Hajj JA. Response of externally post-tensioned continuous members. ACI Structural Journal 2002; 99(5): 671-680.

[20] Aravinthan T, Witchukreangkrai E, Mutsuyoshi H. Flexural behavior of two-span continuous prestressed concrete girders with highly eccentric external tendons. ACI Structural Journal 2005; 102(3): 402-411.

[21] Tan KH, Tjandra RA. Strengthening of RC continuous beams by external prestressing. ASCE Journal of Structural Engineering 2007; 133(2): 195-204.

[22] Lou TJ, Xiang YQ. Finite element modeling of concrete beams prestressed with external tendons. Engineering Structures 2006; 28(14): 1919-1926.

[23] Lou TJ, Lopes SMR, Lopes AV. Nonlinear and time-dependent analysis of continuous unbonded prestressed concrete beams. Computers & Structures 2013; 119: 166-176.

[24] CEN. Eurocode 2: Design of concrete structures – Part 1-1: General rules and rules for buildings. EN 1992-1-1, European Committee for Standardization,

Brussels, Belgium; 2004.

[25] FIB. Model Code 2010. Bulletins 55 and 56, International Federation for Structural Concrete, Lausanne, Switzerland; 2012.

[26] Campbell TI, Chouinard KL. Influence of nonprestressed reinforcement on the strength of unbonded partially prestressed concrete members. ACI Structural Journal 1991; 88(5): 546-551.

[27] Zhou W, Zheng WZ. Experimental research on plastic design method and moment redistribution in continuous concrete beams prestressed with unbonded tendons. Magazine of Concrete Research 2010; 62(1): 51-64.

(a)

(b)
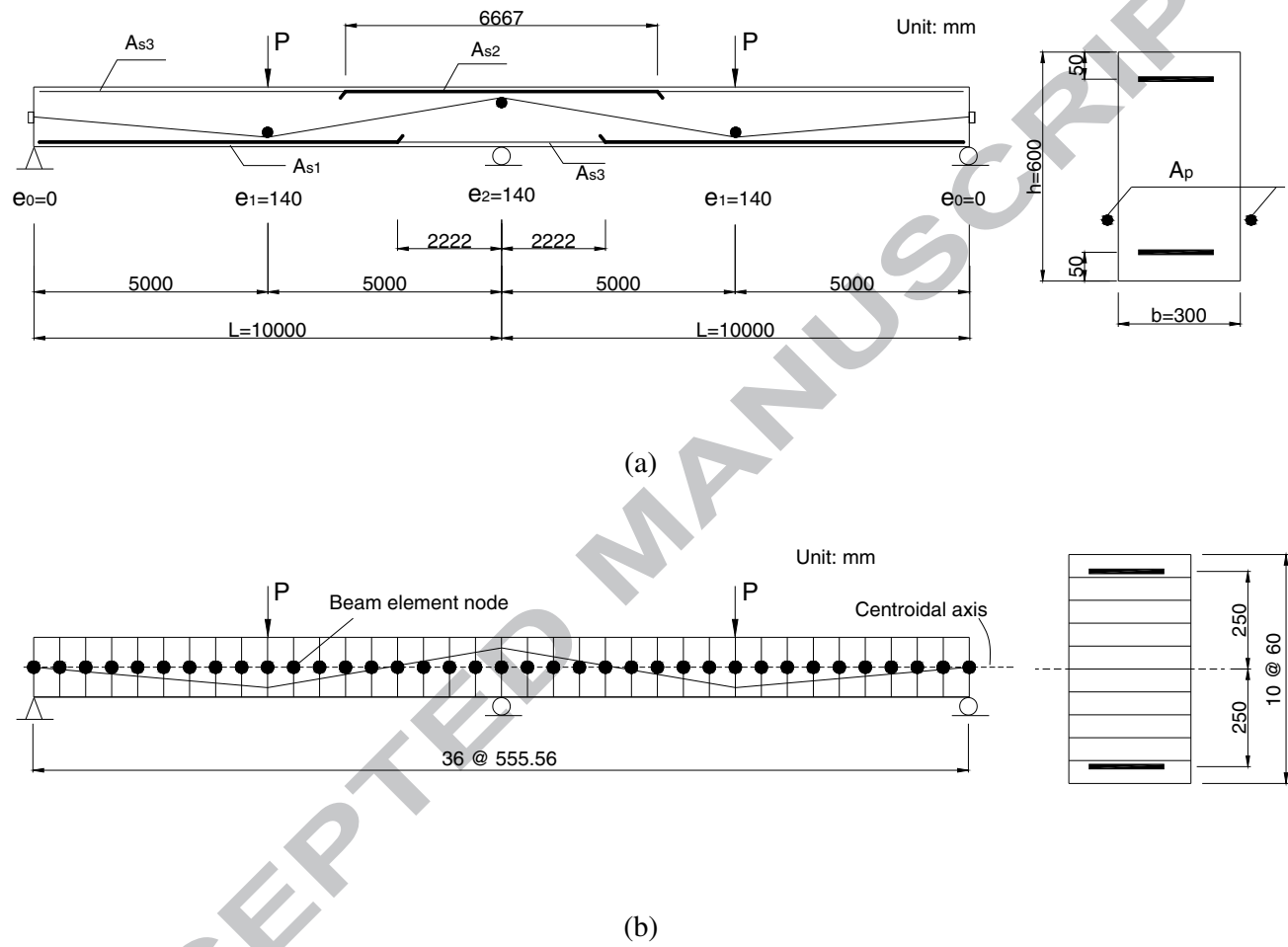
Fig. 1 Control beam for numerical study and its finite element model. (a) beam details;

(b) finite element model
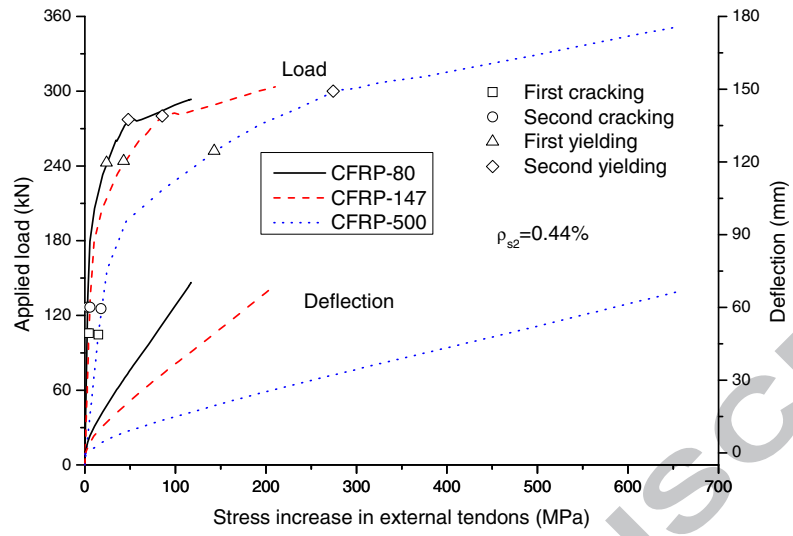
Fig. 2 Stress increase in different types of external CFRP tendons (ρ_{s2} = 0.44%)
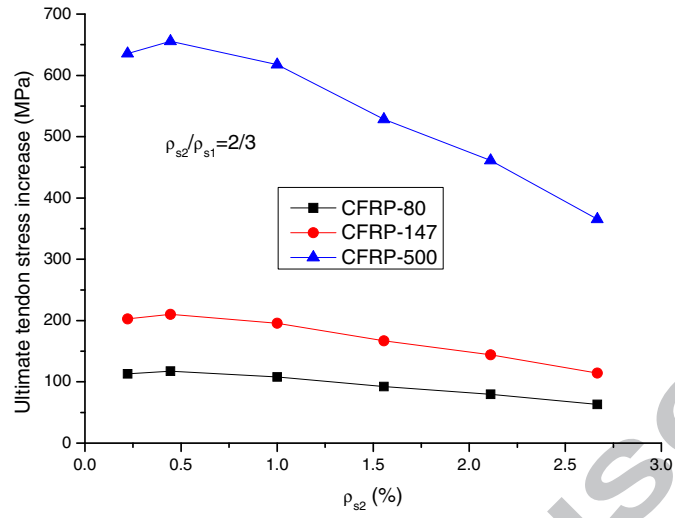
Fig. 3 Variation of ultimate stress increase with steel ratio for different types of

external CFRP tendons
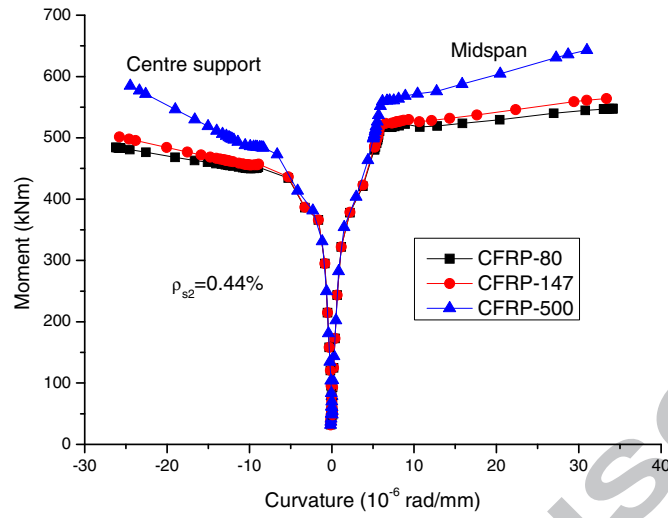
Fig. 4 Moment-curvature response for HSC beams with different types of external

CFRP tendons (ρ_{s2} = 0.44%)
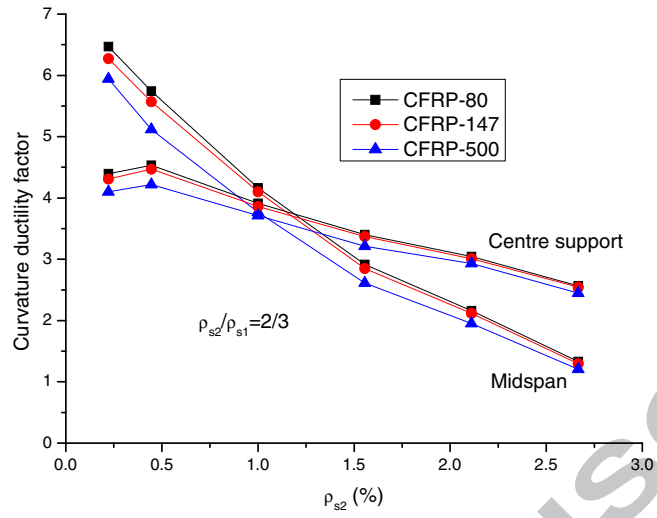
Fig. 5 Variation of curvature ductility factor with steel ratio for HSC beams with

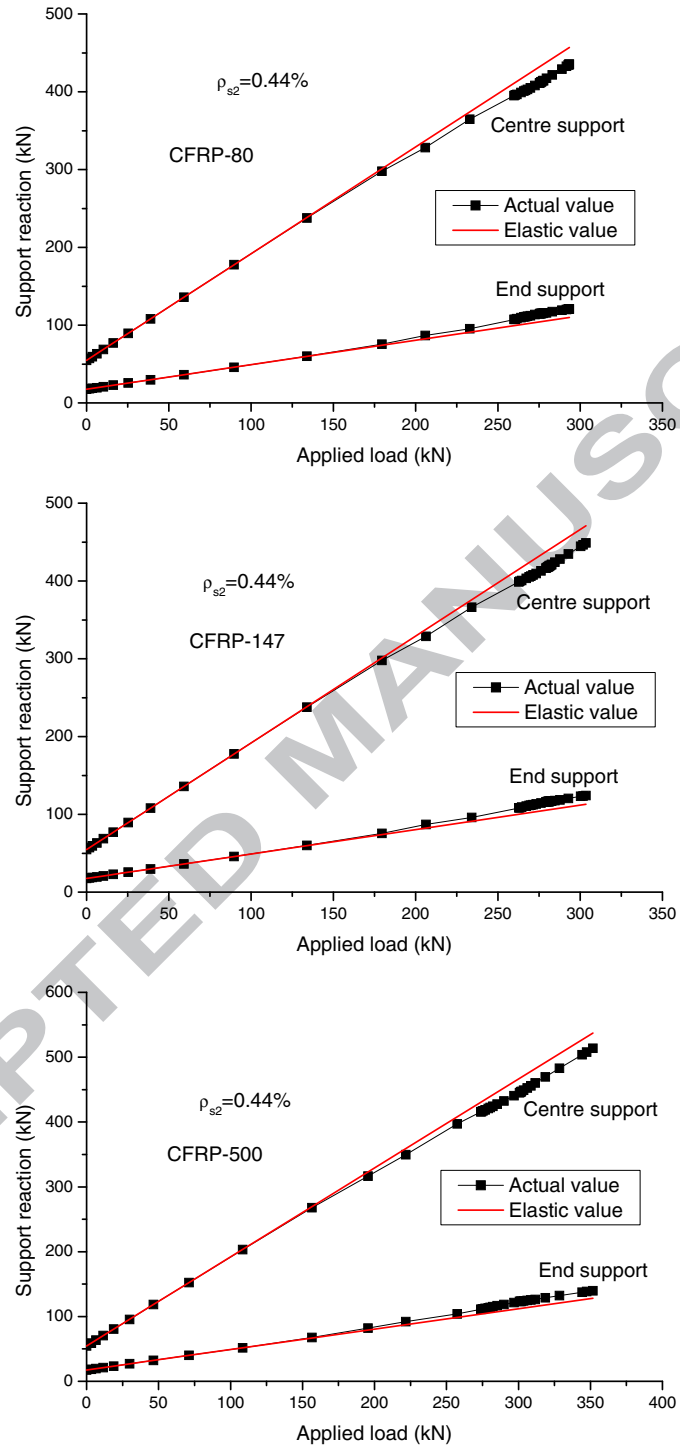different types of external CFRP tendons
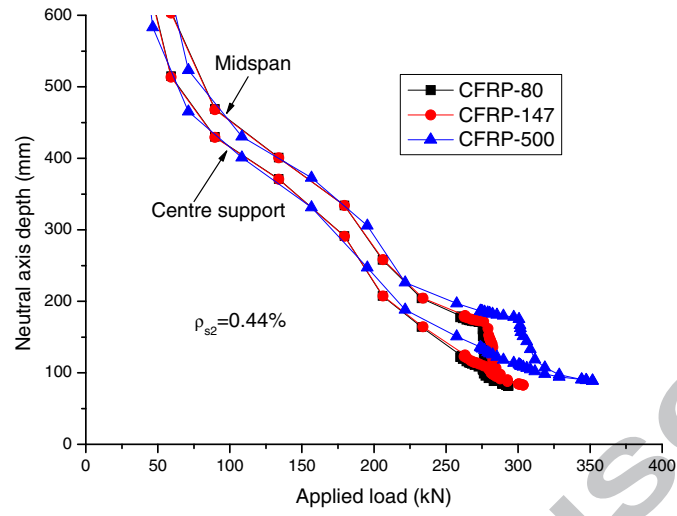
Fig. 6 Variation of neutral axis depth with applied load for HSC beams with different

types of external CFRP tendons (ρ_{s2} = 0.44%)
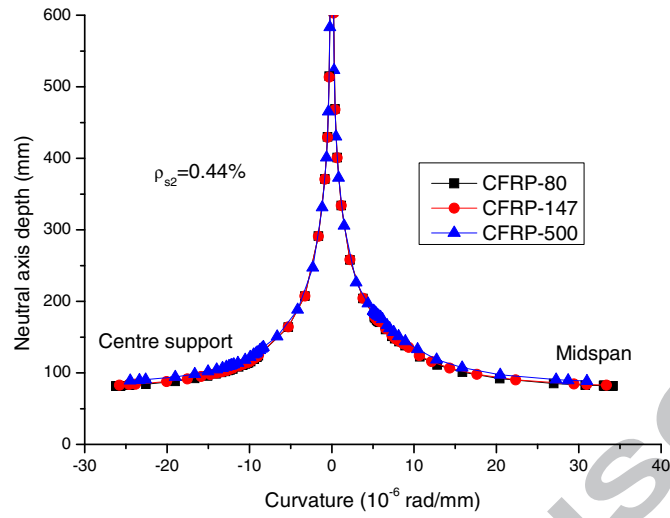
Fig. 7 Variation of neutral axis depth with curvature for HSC beams with different

types of external CFRP tendons (ρ_{s2} = 0.44%)
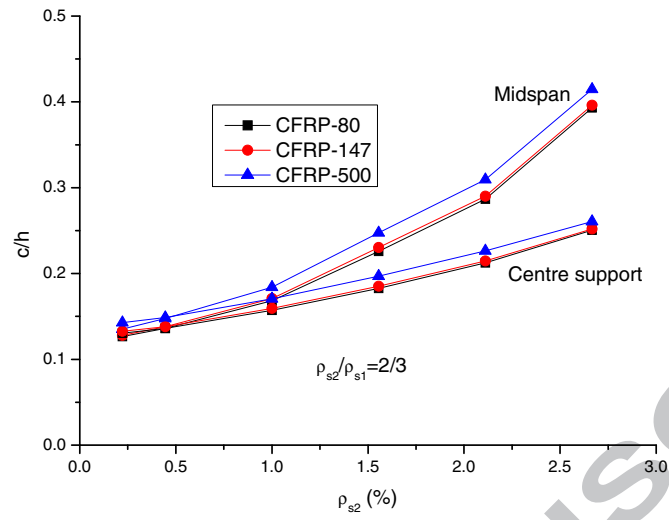
Fig. 8 Variation of c/h with steel ratio for HSC beams with different types of external

CFRP tendons

Fig. 9 Variation of support reaction with applied load for HSC beams with different

types of external CFRP tendons (ρ_{s2} = 0.44%)

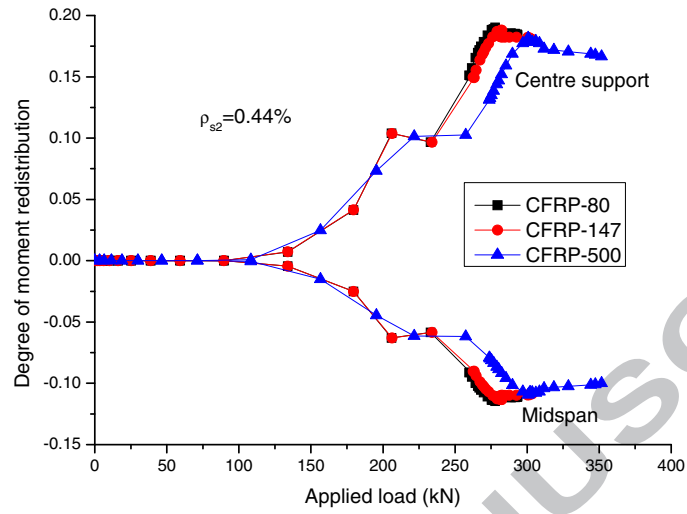Fig. 10 Variation of degree of moment redistribution with applied load for HSC beams

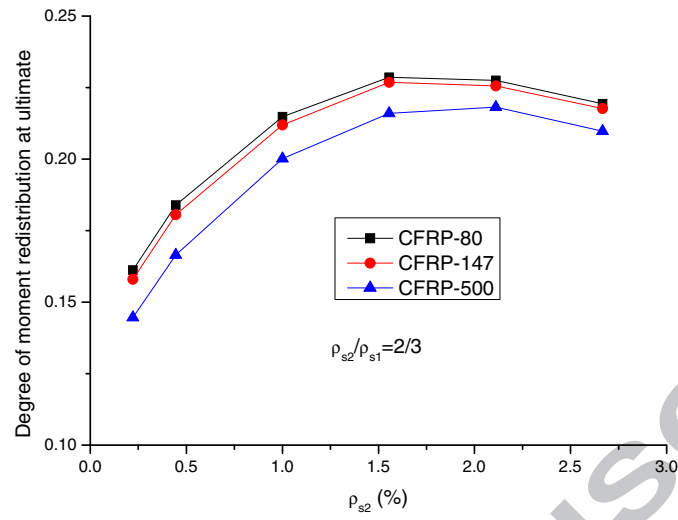with different types of external CFRP tendons (ρ_{s2} = 0.44%)

Fig. 11 Variation of degree of moment redistribution at ultimate with steel ratio for

HSC beams with different types of external CFRP tendons

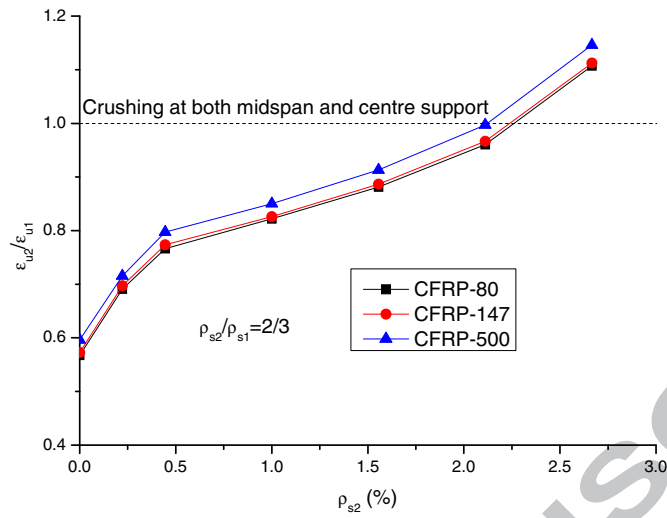Fig. 12 Variation of $\varepsilon_{u2} / \varepsilon_{u1}$ with steel ratio for HSC beams with different types of

external CFRP tendons
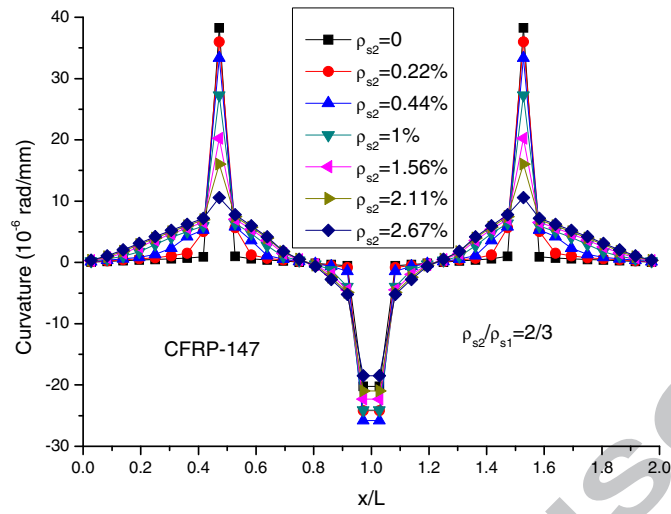
Fig. 13 Curvature distribution along the beam length for beams with various steel
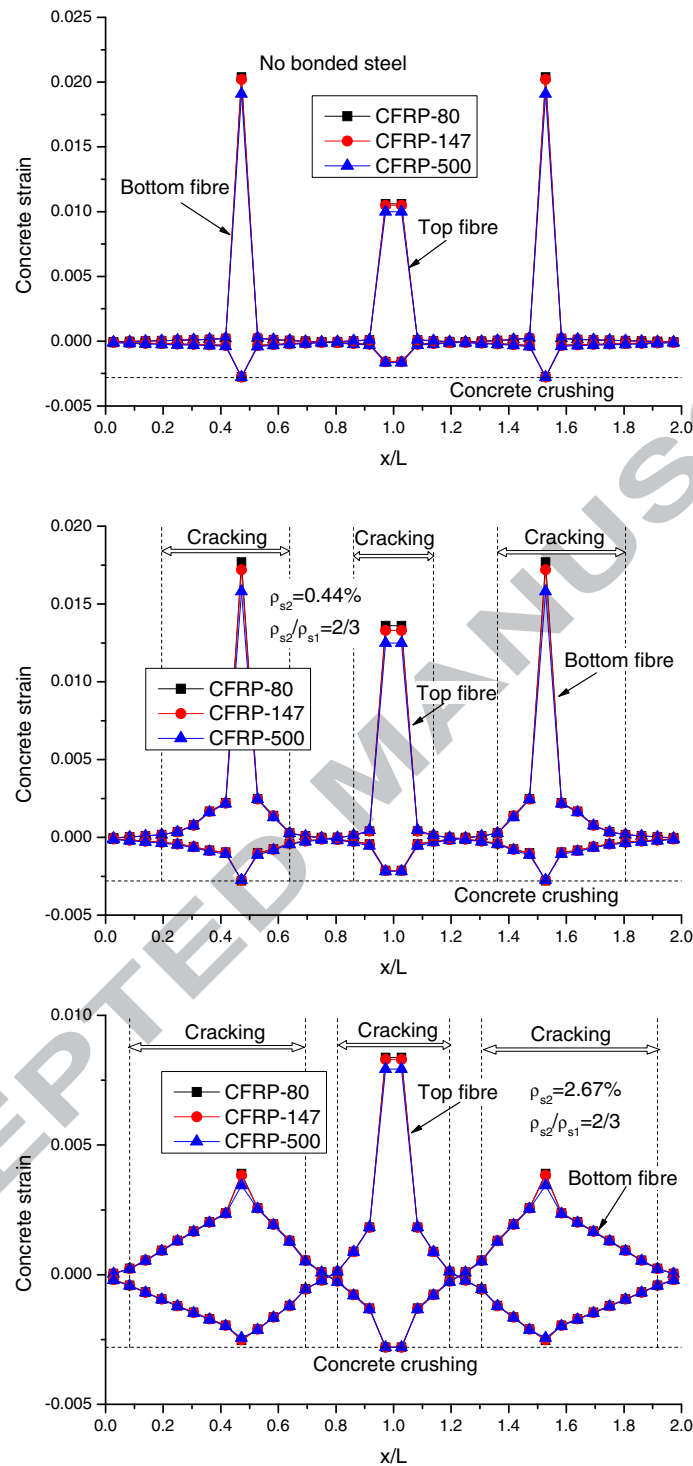
ratio levels

Fig. 14 Concrete strain distribution along the beam length for HSC beams with

different types of external CFRP tendons depending on steel ratio levels

Table 1 Comparison between experimental and computational values of the ultimate

load and tendon stress for the beams tested by Harajli et al. [19]

Beam	Ultimate load			Ultimate tendon stress		
	Test (kN)	Analysis (kN)	Error (%)	Test (MPa)	Analysis (MPa)	Error (%)
B6D1	130.0	130.1	0.1	1492	1494	0.1
B6D2	208.0	202.7	-2.6	1730	1719	-0.6
B12D1	267.0	265.1	-0.7	1242	1414	13.8
B12D2	307.0	311.2	1.4	1439	1551	7.8
B10S1A	191.0	196.0	2.6	1391	1433	3.0
B10S1B	194.0	186.8	-3.7	1304	1424	9.2

Table 2 Mechanical properties for different types of external CFRP tendons

Tendon	f_f (MPa)	E_f (GPa)	ε_{fu} (%)
CFRP-80	1440	80	1.80
CFRP-147	1840	147	1.25
CFRP-500	2500	500	0.5